Turkish Journal of Electrical Engineering & Computer Sciences

http://journals.tubitak.gov.tr/elektrik/

Research Article

Turk J Elec Eng & Comp Sci
()

doi:10.3906/elk-1503-11

Modeling and simulation of sensorless control of four-leg inverter PMSM drives in the case of a single-phase open circuit fault

Kamel SALEH[1,*], **Mark SUMNER**[2]

[1]Department of Electrical Engineering, Faculty of Engineering, An-Najah National University, Nablus, West Bank, Palestine

[2]Department of Electrical and Electronics Engineering, Faculty of Engineering, University of Nottingham, Nottingham, UK

Received: 02.03.2015 • **Accepted/Published Online:** 11.06.2015 • **Final Version:** ..201

Abstract: This paper introduces a new method to track the saliency of a permanent magnet synchronous motor (PMSM) motor fed by a 4-leg inverter in the case of a single-phase open circuit fault through measuring the dynamic current response of the motor line currents due to the insulated-gate bipolar transistor (IGBT) switching actions. In the case of a single-phase open circuit fault, a fault-tolerant control strategy that includes taking appropriate actions to control the 2 remaining healthy currents results in minor system performance degradation. The new strategy introduced in this paper includes software modifications only to the saliency tracking algorithm used in healthy mode in order to make it applicable to the reconfigured converter in the presence of a fault. The new method uses only the fundamental pulse width modulation (PWM) waveform (i.e. there is no modification to the operation of the 4-leg inverter), similar to the fundamental PWM method proposed for a 3-leg inverter. Simulation results are provided to verify the effectiveness of the proposed strategy of saliency tracking of a PMSM motor driven by fault-tolerant 4-phase inverter over a wide range of speeds under the case of a single-phase open circuit fault.

Key words: Four-leg inverter, sensorless, single-phase open circuit, space vector pulse width modulation

1. Introduction

Tracking the saliency of AC motors fed by 2-level 3-leg inverters has been widely researched for healthy mode systems. At low and zero speed, some form of additional excitation has been proposed, such as the injection of a high frequency (HF) voltage or current [1–3] or the injection of test pulses [4–6].

In some applications, such as those in coiling and spooling textile machines and in that of the aerospace and automotive (electric cars) industry, the safety procedures expressly demand a continued operation of the motor drive system after a fault has occurred to reduce the impact of the fault on the system operation. Hence, a number of fault-tolerant strategies for sensored AC motor drives have been used to enhance system operation under open phase faults. The fault-tolerant strategies proposed [7] are based on the connection of either the stator winding neutral point or the motor phase to the DC link middle point of the 2-level 3-leg inverter through a TRIAC. A 2-level 4-leg inverter where the fourth leg is connected to the neutral point of the motor in the case of an open circuit phase fault was proposed [8]. In [9] the fourth leg is connected to the neutral point in healthy and faulty cases and so a 3-dimensional space vector modulation is introduced. A switch function

*Correspondence: kamel.saleh@najah.edu

algorithm for a 4-leg converter to synthesize redefined output waveforms under fault conditions was proposed in [10]. However, approaches to track the saliency in the fault-tolerant inverters have received little attention in the literature.

This paper proposes a fault-tolerant, 4-phase inverter permanent magnet synchronous motor (PMSM) drive topology that can be used to track the saturation saliency in permanent magnet (PM) motors and rotor slotting saliency in induction motors (IMs) in the case of single-phase open circuit faults in order to maintain continuous system operation with a satisfactory performance to meet the safety procedure for the whole system and increase the reliability of the system.

2. Fault tolerant 2-level 4-leg converter drive topology

Figure 1 shows the proposed fault-tolerant 2-level 4-leg converter drive topology [11–17]. In this topology, a fourth leg is added to the conventional 3-leg inverter and the redundant leg is permanently connected to the motor neutral point to provide the fault-tolerant capability in the case of an open phase fault. Under healthy operating conditions, the fourth leg will be redundant, which means that the 2 switches in this leg will be inactivated, resulting in no connection between the supply and the motor neutral point. Therefore, the proposed converter normally operates as a conventional 2-level 3-leg inverter. Under faulted operating conditions, the switches on the faulty phase are disabled and the switches in the fourth phase are immediately activated in order to control the voltage at the neutral point of the motor.

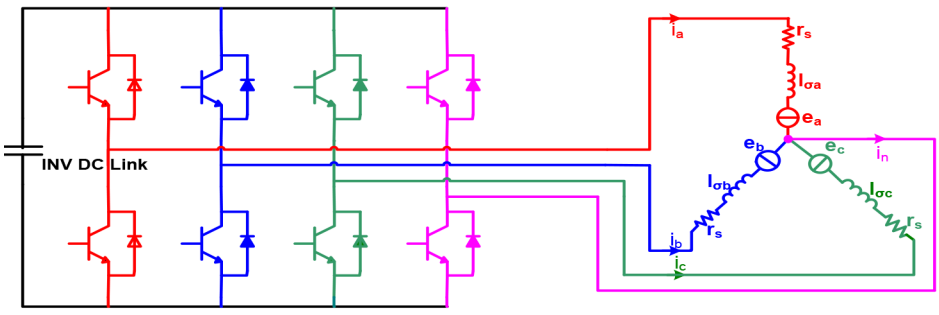

Figure 1. The fault-tolerant 2-level 4-leg converter motor drive configuration.

3. Sensored control strategy for the fault-tolerant motor drive

Indirect vector control is employed to control the speed of the motor in both normal and faulted operating conditions.

3.1. Normal operating condition in sensored mode

Figure 2 shows the vector control structure used for the 2-level 4-leg inverter motor drive under normal operation in sensored mode. The 3-phase motor currents are transformed to the d-q synchronous rotating frame, id and iq, as given in Eq. (1) to compare to the reference values. The reference voltages (Vd and Vq) generated from the controller are transformed back, using Eq. (2), to 3-phase quantities, which are then delivered to the space vector modulator to generate the appropriate switching signals for the fault tolerant inverter switches.

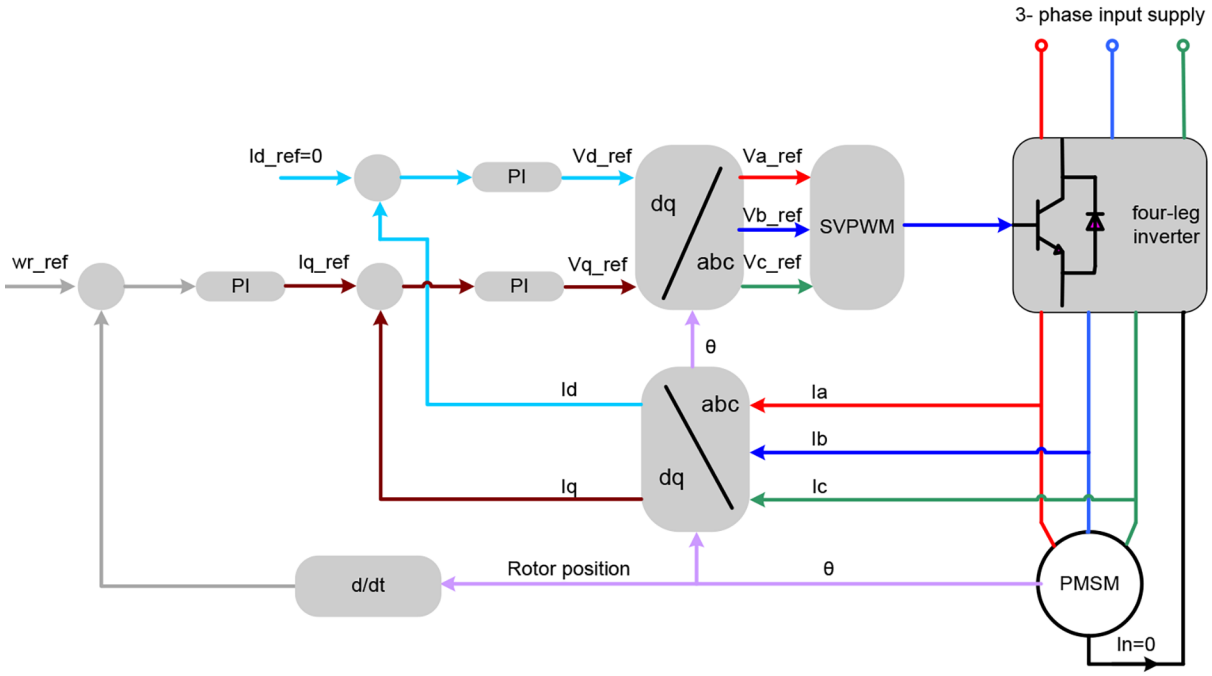

Figure 2. Control structure of 4-leg PMSM drive under healthy operating conditions.

$$\begin{bmatrix} Iq \\ Id \\ I0 \end{bmatrix} = \frac{2}{3} \begin{bmatrix} cos(\theta) & cos(\theta-120) & cos(\theta+120) \\ sin(\theta) & sin(\theta-120) & sin(\theta+120) \\ 0.5 & 0.5 & 0.5 \end{bmatrix} \begin{bmatrix} Ia \\ Ib \\ Ic \end{bmatrix} \tag{1}$$

$$\begin{bmatrix} Va \\ Vb \\ Vc \end{bmatrix} = \begin{bmatrix} cos(\theta) & sin(\theta) & 1 \\ cos(\theta-120) & sin(\theta-120) & 1 \\ sin(\theta-120) & sin(\theta+120) & 1 \end{bmatrix} \begin{bmatrix} Vq \\ Vd \\ V0 \end{bmatrix} \tag{2}$$

Here, θ is the rotor angle of the reference frame. I0 is the zero sequence current while In is the motor neutral current as expressed in Eqs. (1) and (2), respectively. Under normal operation the neutral current is always zero.

3.2. Open phase fault operation

The modification introduced to the control strategy of the system under open phase fault condition is illustrated in Figure 3 [12–17]. First, in order to disable the switches in the faulty phase, the reference voltage of the faulty phase is set to zero. In this structure, it is assumed that phase a is opened so the motor current in phase a drops to zero and Va_ ref is set to zero, whereas the motor neutral current, which is the sum of the two remaining output currents (Ib and Ic), can circulate through the fourth phase of the inverter. Secondly, by adopting Ia $=$ 0 in Eq. (1), it can be seen that in order to keep the motor performance under faulty operation, the rotating magnetomotive force obtained from the armature currents (Ia, Ib, Ib) in the healthy condition should be maintained by the two remaining motor currents (Ib, Ic) in the case of an open circuit fault that demands an increase of $\sqrt{3}$ as well as phase shifting 30 degrees away from the faulted phase compared to the currents generated under normal operation, as given in Eq. (3).

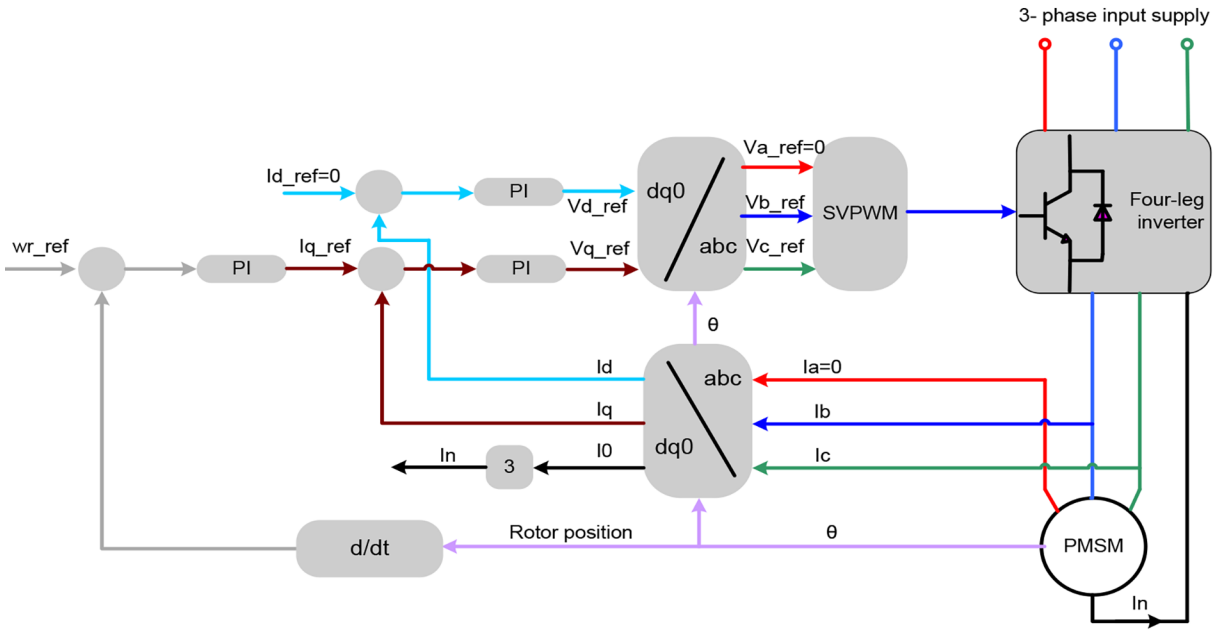

Figure 3. The vector control structure for the 4-phase inverter PMSM drive under a phase a open-circuit fault.

$$\begin{bmatrix} I0 \\ Ib \\ Ic \end{bmatrix} = \begin{bmatrix} -cos(\theta) & -sin(\theta) \\ \sqrt{3}cos(\theta - 150) & \sqrt{3}sin(\theta - 150) \\ \sqrt{3}sin(\theta - 150) & \sqrt{3}sin(\theta + 150) \end{bmatrix} \begin{bmatrix} Vq \\ Vd \end{bmatrix} \tag{3}$$

3.3. Simulation results

The simulation of a 4-leg converter PMSM drive was carried out using SABER. A 5 Nm load torque and a 500 rpm speed command are applied to the system. Figure 4 shows the simulation results of the 4-leg converter PMSM drive system under healthy and faulted conditions. It is clear that the controller could regulate the motor speed to follow the reference speed properly under normal operating conditions. The controlled currents id and iq are stable at the reference levels while the motor currents are balanced 3-phase sinusoidal. The phase a open circuit fault is introduced at the time of 2.5 s. As the switches in the fourth leg of the inverter are not activated yet, then In = 0, and I0 = 0, and as the sum of the 3 currents equals zero then Ib and Ic currents increase in magnitude with phase shifting 180 degrees with respect to each other. In this period a significant ripple in Id and Iq can be seen, which leads to a significant ripple in torque and speed. At 3.0 s, the switch of the fourth leg is activated, which means that the neutral is connected to the supply. The simulation results show that ripple in the torque is significantly reduced and almost the same as under normal operating conditions. The currents id and iq are now controlled properly

4. Tracking the saturation saliency of the PMSM under healthy conditions

The stator leakage inductances of the induction motor are modulated by anisotropy either from the rotor slotting or from the saturation of the main flux. The modulation can be expressed by the following equations:

$$l\sigma a = L_0 + \Delta L cos\left(n_{an}\theta_{an}\right) \tag{4}$$

$$l\sigma b = L_0 + \Delta L cos\left(n_{an}(\theta_{an} - \frac{2\pi}{3}\right) \tag{5}$$

$$l\sigma c = L_0 + \Delta L cos\left(n_{an}(\theta_{an} - \frac{4\pi}{3}\right) \tag{6}$$

Here, L_0 is the average inductance and ΔL is the variation of leakage inductance due to the rotor anisotropy ($n_{an} = 2$ for saturation anisotropy).

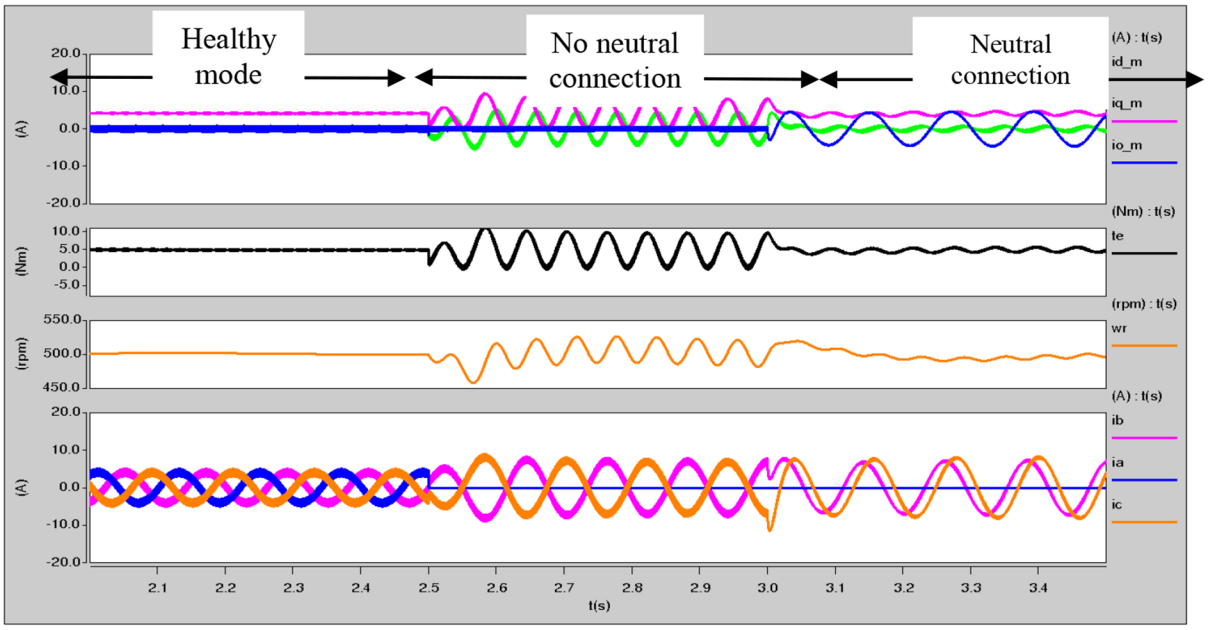

Figure 4. Performance of a 4-phase direct matrix converter PMSM drive system under different operating conditions.

This modulation of the stator leakage inductances will be reflected in the transient response of the motor line current to the test vector imposed by the inverter. Thus, by using the fundamental pulse width modulation (PWM) wave form and by measuring the transient current response to the active vectors it is possible to detect the inductance variation and track the rotor position as shown in [6] for a 3-leg inverter. Figure 5a, Figure 5b, and Table 1 illustrate this method

After obtaining the scalar quantities pa, pb, and pc, then the position of saliency can be constructed as shown in the equation below:

$$\vec{p} = p_\alpha + jp_\beta = p_a + ap_b + a^2 p_c \tag{7}$$

For a 4-leg inverter, under healthy operation, the switches in the fourth leg will not be activated so the algorithm proposed in [6] to track the saliency for a 3-leg inverter PMSM drive system can be applied for the 4-leg inverter PMSM drive system as shown in Figure 6. In an open phase fault case, the measurement of the current response (di/dt) associated with the faulty phase will become zero, i.e. $\frac{di_a}{dt}^{V1}, \frac{di_a}{dt}^{V2}, and \frac{di_a}{dt}^{V0}$ become zeros as ia = 0. Table 1 shows that Pa is obtained using $\frac{di_a}{dt}$ in sectors 1 and 4, Pb is obtained using $\frac{di_a}{dt}$ in sectors 2 and 5, and Pc is obtained using $\frac{di_a}{dt}$ in sectors 3 and 6, which means that these position scalars will be zero in these sectors,

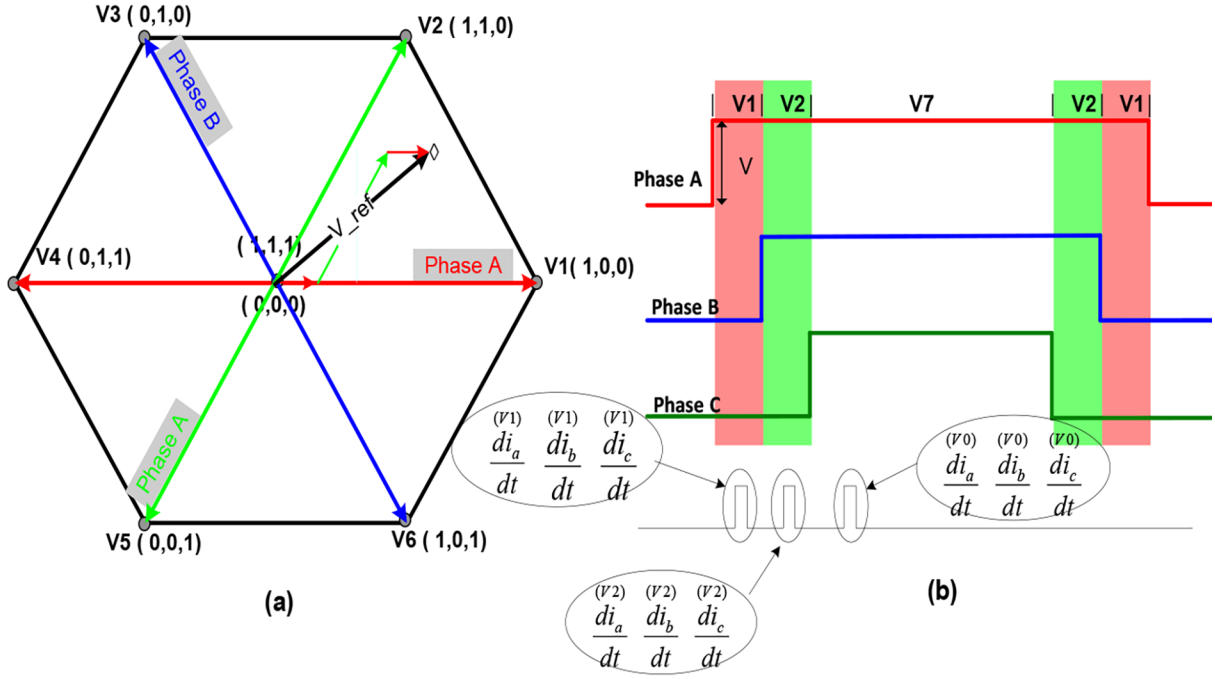

Figure 5. SVPWM modulation technique of 3-leg inverter in healthy mode: (a) definition of space vectors; (b) switching patterns (waveforms) in the first sector.

Table 1. Selection of pa, pb, and pc in 6 sectors for a star-connected machine using fundamental PWM method.

	P_a	P_b	P_c
V1 + V0	$2-c(\frac{di_a^{(V1)}}{dt}-\frac{di_a^{(V0)}}{dt})$	$-1-c(\frac{di_c^{(V1)}}{dt}-\frac{di_c^{(V0)}}{dt})$	$-1-c(\frac{di_b^{(V1)}}{dt}-\frac{di_b^{(V0)}}{dt})$
V2 + V0	$-1+c(\frac{di_b^{(V2)}}{dt}-\frac{di_b^{(V0)}}{dt})$	$-1+c(\frac{di_a^{(V2)}}{dt}-\frac{di_a^{(V0)}}{dt})$	$2+c(\frac{di_c^{(V2)}}{dt}-\frac{di_c^{(V0)}}{dt})$
V3 + V0	$-1-c(\frac{di_c^{(V3)}}{dt}-\frac{di_c^{(V0)}}{dt})$	$2-c(\frac{di_b^{(V3)}}{dt}-\frac{di_b^{(V0)}}{dt})$	$-1-c(\frac{di_a^{(V3)}}{dt}-\frac{di_a^{(V0)}}{dt})$
V4 + V0	$2+c(\frac{di_a^{(V4)}}{dt}-\frac{di_a^{(V0)}}{dt})$	$-1+c(\frac{di_c^{(V4)}}{dt}-\frac{di_c^{(V0)}}{dt})$	$-1+c(\frac{di_b^{(V4)}}{dt}-\frac{di_b^{(V0)}}{dt})$
V5 + V0	$-1-c(\frac{di_b^{(V5)}}{dt}-\frac{di_b^{(V0)}}{dt})$	$-1-c(\frac{di_a^{(V5)}}{dt}-\frac{di_a^{(V0)}}{dt})$	$2-c(\frac{di_c^{(V5)}}{dt}-\frac{di_c^{(V0)}}{dt})$
V6 + V0	$-1+c(\frac{di_c^{(V6)}}{dt}-\frac{di_c^{(V0)}}{dt})$	$2+c(\frac{di_b^{(V6)}}{dt}-\frac{di_b^{(V0)}}{dt})$	$-1+c(\frac{di_a^{(V6)}}{dt}-\frac{di_a^{(V0)}}{dt})$

as seen in Figure 6. Moreover, the active vectors V1, V2, and V0 in each sector will not be obtained by applying specific switching actions in phase a, b, and c as in the healthy case as there will not be any switching action in phase a due to the fault. Hence, the tracking saliency algorithm will be incorrect, as shown in Figure 6.

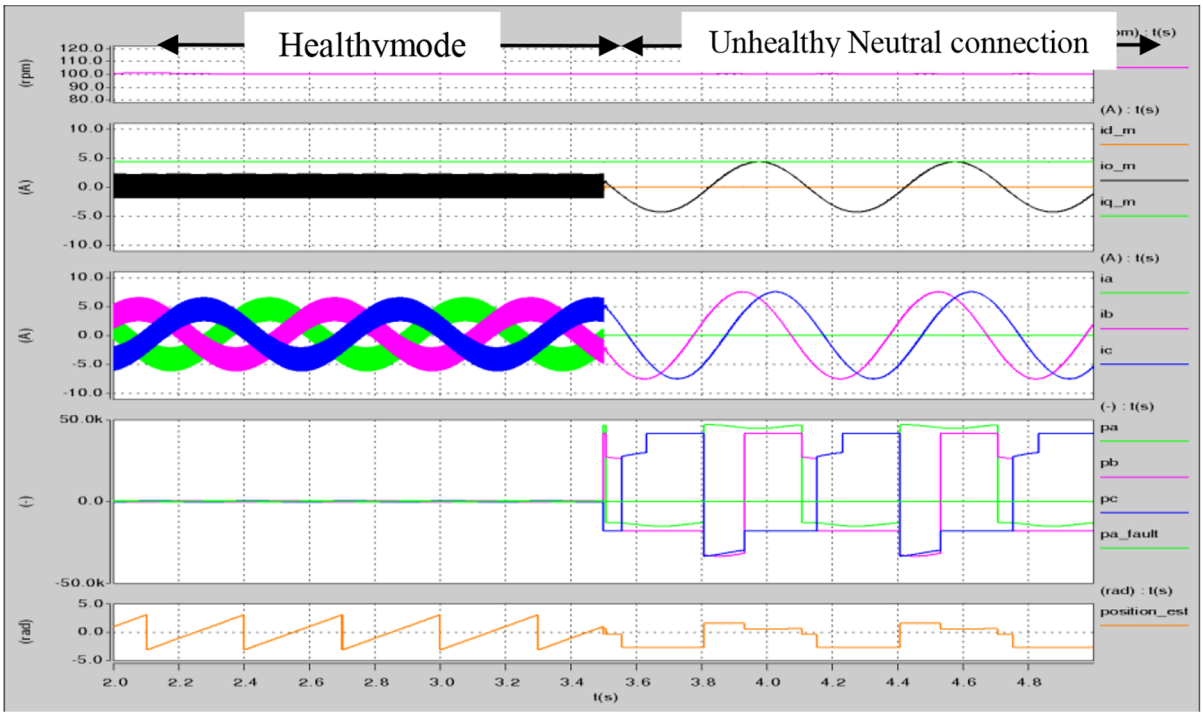

Figure 6. Tracking the saliency saturation in healthy mode and phase a open circuit case.

5. Tracking the saturation saliency of the PMSM under unhealthy conditions

Figure 6 shows that the algorithm presented in [6] to track the saliency cannot be used in the case of a phase open circuit. In this section a modified algorithm will be applied to track the saliency in the case of an open circuit fault using the current response of application of fundamental PWM waveform (no modification applied to the PWM waveform). The new algorithm uses only the current response of an application of fundamental PWM wave form of healthy phases to track the saliency and does not use the current response of the open circuit phase as it will be zero. After measuring the current response of the 2 healthy phases according to the sector number of the space vector modulation state diagram that the reference voltage exists in, the 3 position scalars quantities can be deduced and hence the saliency position can be obtained.

Figure 7a and Figure 7b show the space vector modulation state diagram for a 4-leg inverter in the case of an open circuit phase fault case. If V_ ref exists in the first sector, then the switching sequences and the timing of the applied vectors will be as shown in Figure 7b.

The stator circuit when vectors V1, V2, and V0 are applied are shown in Figure 8a, Figure 8b, and Figure 8c, respectively.

Using the circuit in Figure 8a, the following equations hold true:

$$-V_{DC} = r_s * i_b{}^{(V1)} + l_{\sigma b} * \frac{di_b^{(V1)}}{dt} + e_b^{(V1)} \tag{8}$$

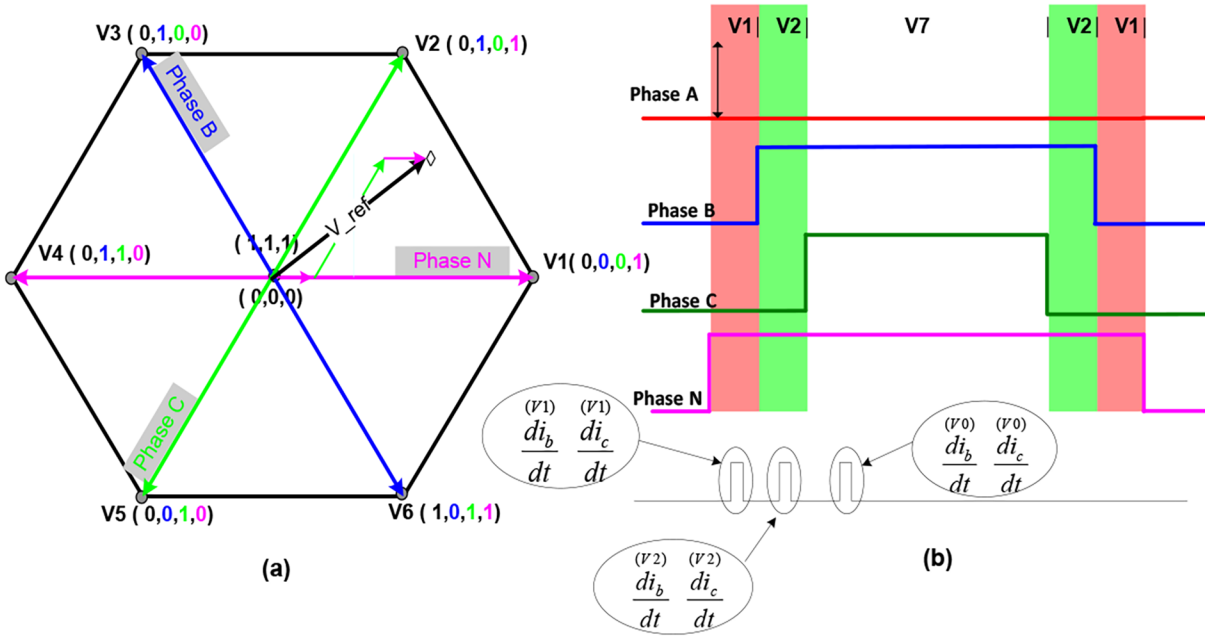

Figure 7. SVPWM modulation technique in phase a open circuit fault case: (a) definition of space vectors; (b) switching patterns (waveforms) in the first sector.

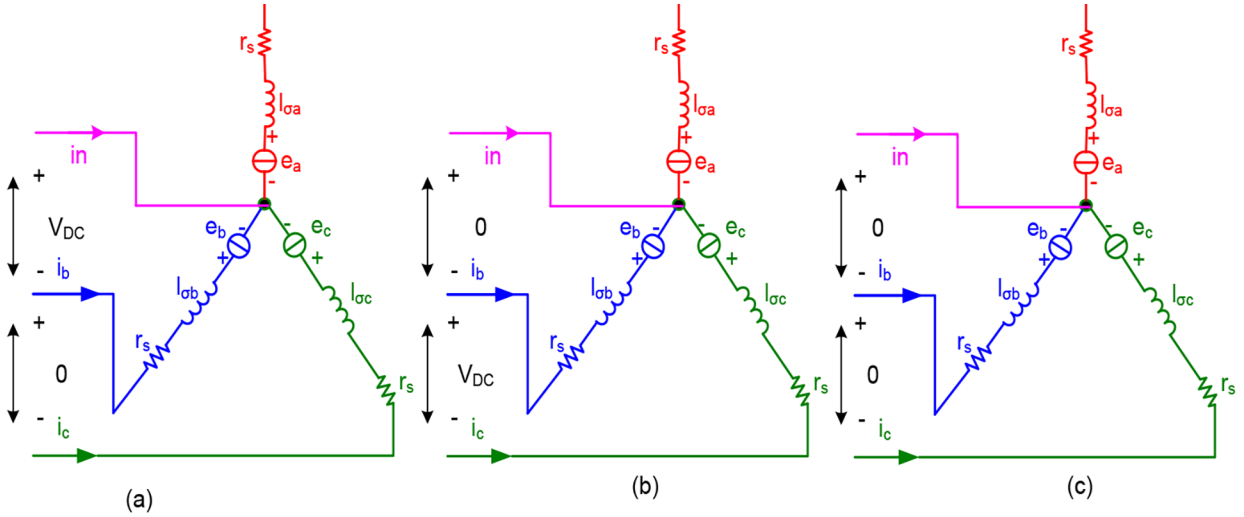

Figure 8. Stator circuits when: (a) V1 is applied; (b) V2 is applied; (c) V0 is applied under phase a open circuit fault.

$$-V_{DC} = r_s * i_c{}^{(V1)} + l_{\sigma c} * \frac{di_c^{(V1)}}{dt} + e_c^{(V1)} \tag{9}$$

The following equations are obtained using Figure 8b:

$$0 = r_s * i_b{}^{(V2)} + l_{\sigma b} * \frac{di_b^{(V2)}}{dt} + e_b^{(V2)} \tag{10}$$

$$-V_{DC} = r_s * i_c{}^{(V2)} + l_{\sigma c} * \frac{di_c^{(V2)}}{dt} + e_c^{(V2)} \tag{11}$$

Finally, when V0 is applied as shown in Figure 8c, the following equations hold true:

$$0 = r_s * {i_b}^{(V0)} + l_{\sigma b} * \frac{di_b^{(V0)}}{dt} + e_b^{(V0)} \tag{12}$$

$$0 = r_s * {i_c}^{(V0)} + l_{\sigma c} * \frac{di_c^{(V0)}}{dt} + e_c^{(V0)} \tag{13}$$

We assume that the voltage drops across the stator resistances are small and can be neglected and the back electromotive force can be cancelled if the time separation between the vectors is small.

Subtracting Eqs. (10) and (13) from Eqs. (8) and (11) respectively yields:

$$V_{DC} = l_{\sigma b} * (\frac{di_b^{(V2)}}{dt} - \frac{di_b^{(V1)}}{dt}) \tag{14}$$

$$V_{DC} = l_{\sigma c} * \left(\frac{di_c^{(V0)}}{dt} - \frac{di_c^{(V2)}}{dt} \right) \tag{15}$$

Finally:

$$Pb = \left(\frac{di_b^{(V2)}}{dt} - \frac{di_b^{(V1)}}{dt} \right) \tag{16}$$

$$Pc = \left(\frac{di_c^{(V0)}}{dt} - \frac{di_c^{(V2)}}{dt} \right) \tag{17}$$

Pa cannot be obtained from measuring the current response in phase a as it is zero in the case of an open circuit phase, but it can be deduced from pb and pc according to the following equation:

$$Pa = -pb - pc \tag{18}$$

By doing the same procedures for other sectors, tables can be construct.

Figure 9 shows the results of the simulation after modifying the tracking saliency algorithm as in Table 2. The figure shows that the new algorithm can track the saliency in the case of an open circuit phase a fault with the same quality as in healthy conditions.

6. Fully sensorless speed control

The position and speed control for a PM machine have been implemented in simulation in the SABER modeling environment. The estimated position signals P$\alpha\beta$ from the equations selected are used as the input to a mechanical observer [17] to obtain the speed $\omega^{\wedge}$ and a cleaned position $\theta^{\wedge}$. Note that the simulation includes a minimum pulse width of 10 mu s when di/dt measurements are made, similar to the experimental results of [6]. This estimated speed $\omega^{\wedge}$ and position $\theta^{\wedge}$are used to obtain a fully sensorless speed control as shown in Figure 10.

Figure 11 shows the results of a fully sensorless speed control of a PMSM motor driven by a 4-leg inverter at loaded conditions using the algorithm proposed in [6] for the healthy case and the method proposed above in

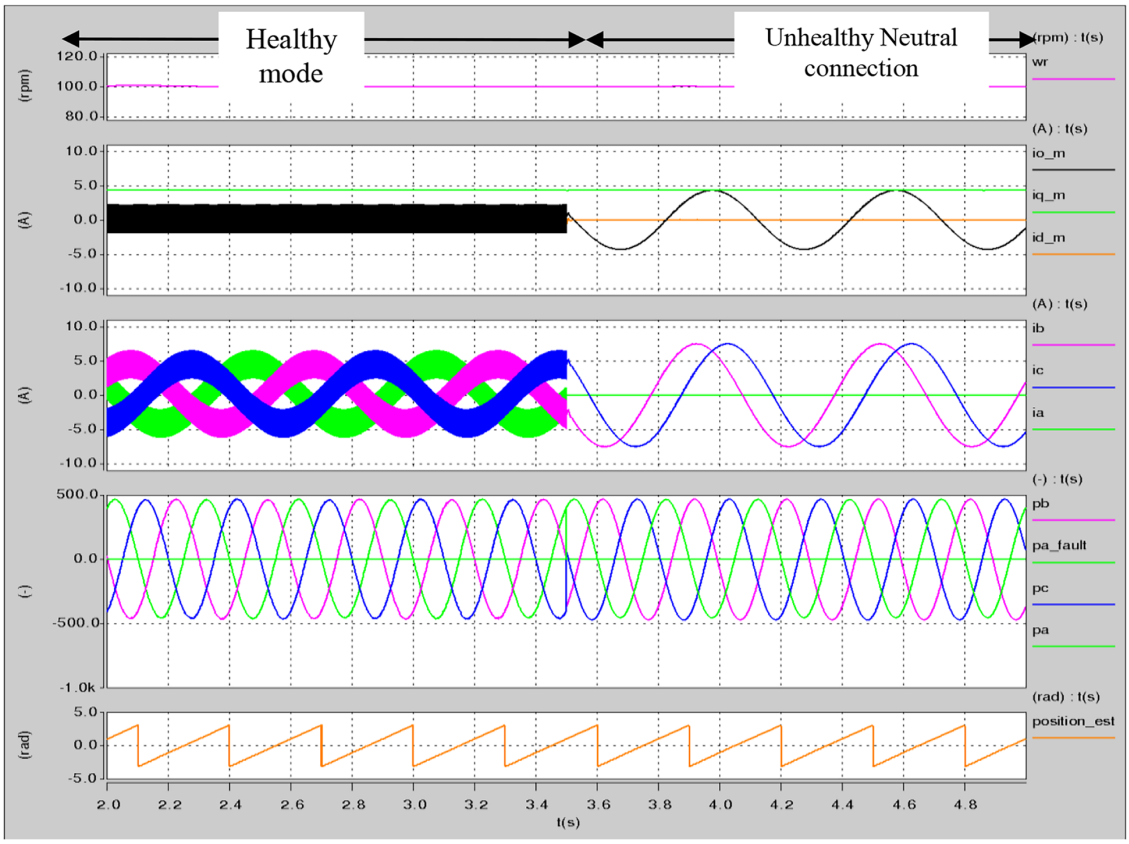

Figure 9. Tracking the saliency saturation in healthy mode and phase a open circuit case using the new algorithm.

Table 2. Selection of pa, pb, and pc for a star-connected machine in phase a open circuit fault case.

	P_a	P_b	P_c
V1 + V2 + V0	$-P_b - P_c$	$(\frac{di_b}{dt}^{(V2)} - \frac{di_b}{dt}^{(V1)})$	$(\frac{di_c}{dt}^{(V0)} - \frac{di_c}{dt}^{(V2)})$
V2 + V3 + V0	$-P_b - P_c$	$(\frac{di_b}{dt}^{(V3)} - \frac{di_b}{dt}^{(V0)})$	$(\frac{di_c}{dt}^{(V0)} - \frac{di_c}{dt}^{(V2)})$
V3 + V4 + V0	$-P_b - P_c$	$(\frac{di_b}{dt}^{(V3)} - \frac{di_b}{dt}^{(V0)})$	$(\frac{di_c}{dt}^{(V4)} - \frac{di_c}{dt}^{(V3)})$
V4 + V5 + V0	$-P_b - P_c$	$(\frac{di_b}{dt}^{(V5)} - \frac{di_b}{dt}^{(V4)})$	$(\frac{di_c}{dt}^{(V4)} - \frac{di_c}{dt}^{(V5)})$
V5 + V6 + V0	$-P_b - P_c$	$(\frac{di_b}{dt}^{(V0)} - \frac{di_b}{dt}^{(V6)})$	$(\frac{di_c}{dt}^{(V5)} - \frac{di_c}{dt}^{(V0)})$
V6 + V1 + V0	$-P_b - P_c$	$(\frac{di_b}{dt}^{(V0)} - \frac{di_b}{dt}^{(V6)})$	$(\frac{di_c}{dt}^{(V6)} - \frac{di_c}{dt}^{(V5)})$

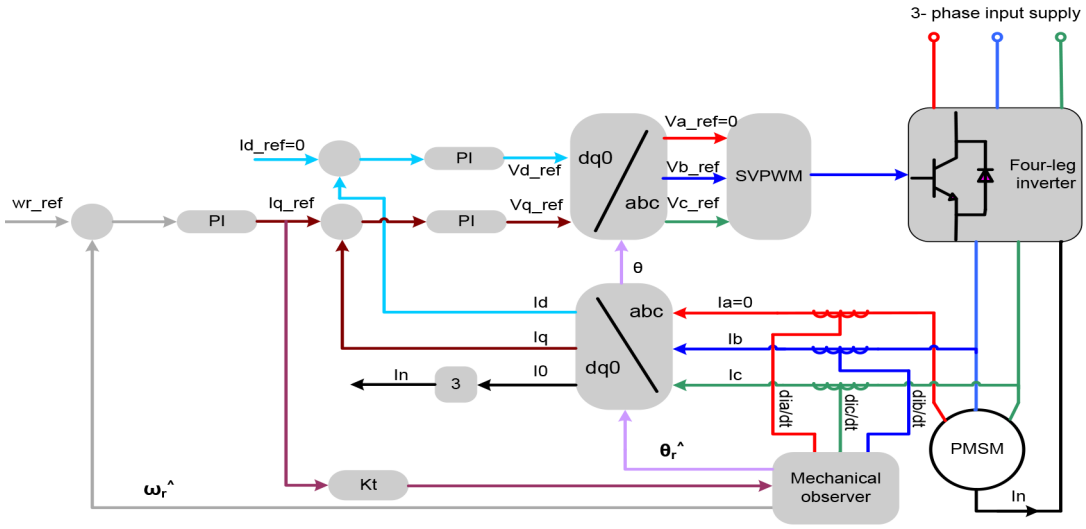

Figure 10. The sensorless vector control structure for the 4-phase inverter PMSM drive under a phase a open-circuit fault.

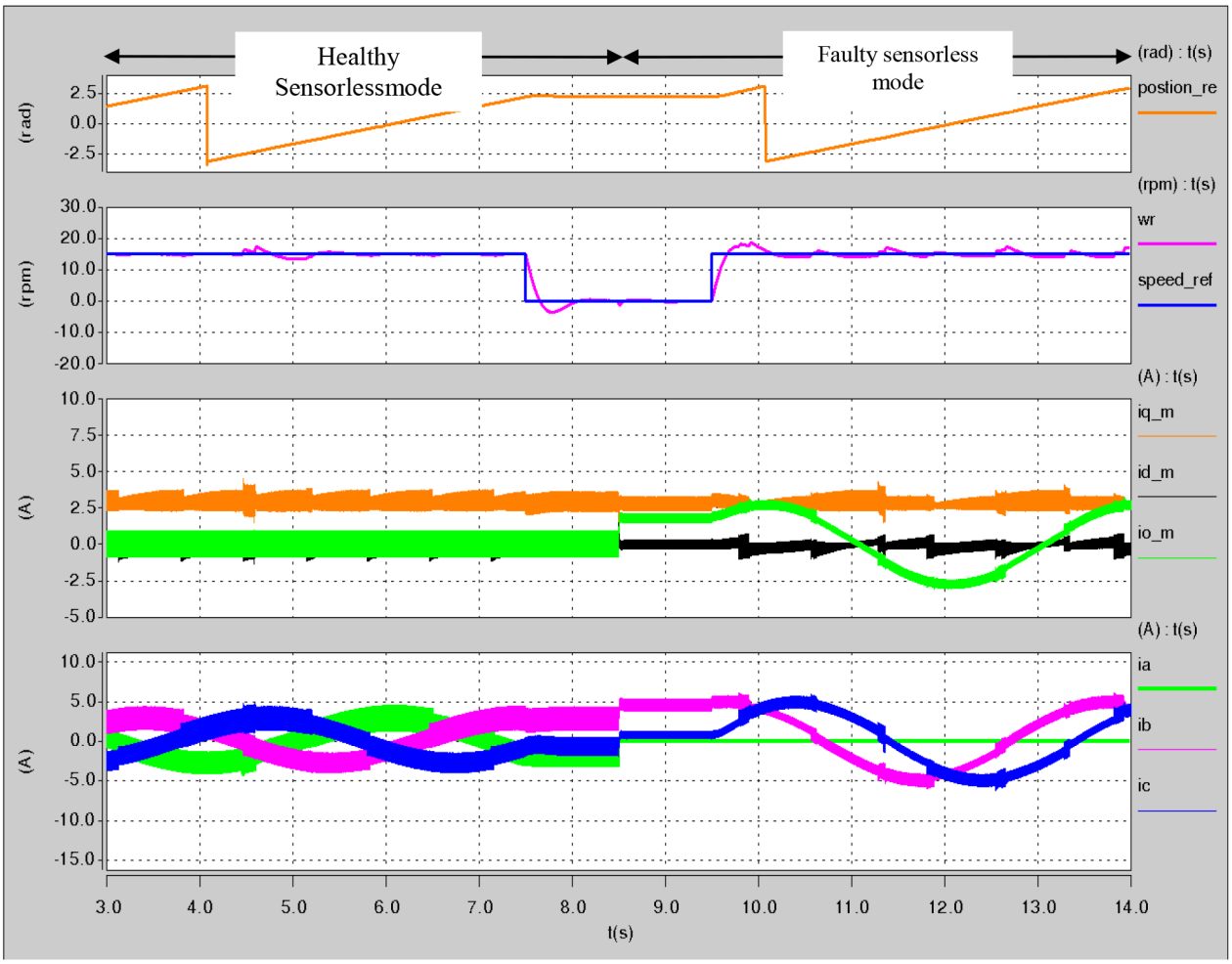

Figure 11. Fully sensorless speed steps between 0.5 Hz, 0 to 0.5 Hz, half under healthy condition and half under open phase a fault condition.

the case of open circuit fault condition. The motor was working in sensorless healthy mode at speed = 0.5 Hz, and then at time t = 7.5 s a speed step change from 0.5 Hz to 0 rpm (until t = 8.5 s) is applied to the system. Figure 11 shows that the motor responded to the speed step with a good transient and steady state response. Moreover, as the motor is in healthy mode, In = 0 and the current is 3 balanced sinusoidal wave forms when speed_ ref = 0.5 Hz. At time t = 8.5 s, an open circuit fault in phase a was introduced to the system, and this can be noticed from In #0 and the current waveforms (Ia = 0, Ib, and Ic are multiplied by $\sqrt{3}$ and shifted by 60 degrees). Figure 11 shows that performance of the whole system under faulty conditions is in the same level of performance in healthy mode. Moreover, the motor responded to a speed step from 0 to 0.5 Hz at t = 10.5 s with acceptable transient and steady state performance.

Figure 12 shows results similar to results shown in Figure 11 but with higher speed steps commanded from the system. The figure shows the effectiveness of the system in response to the high speed steps (from 10 Hz to 0 back to 10 Hz) in the healthy case as well as the case of an open circuit in phase a.

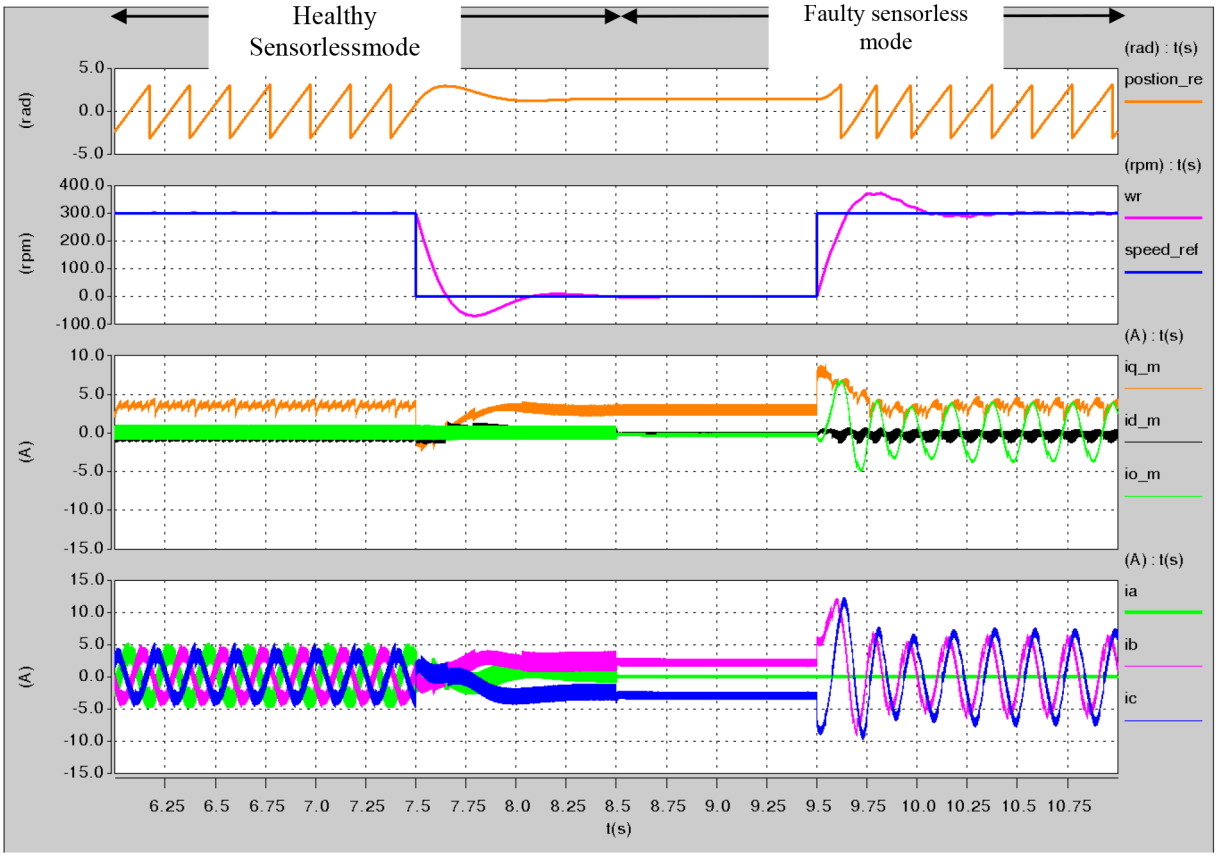

Figure 12. Fully sensorless speed steps between 10 Hz, 0 to 10 Hz, half under healthy condition and half under open phase a fault condition.

Figure 13 demonstrates the stability of the fully sensorless system when a load disturbance is applied at low speed (1 Hz) in both healthy mode and under open phase fault conditions. The results show that the system maintains the speed in all the cases.

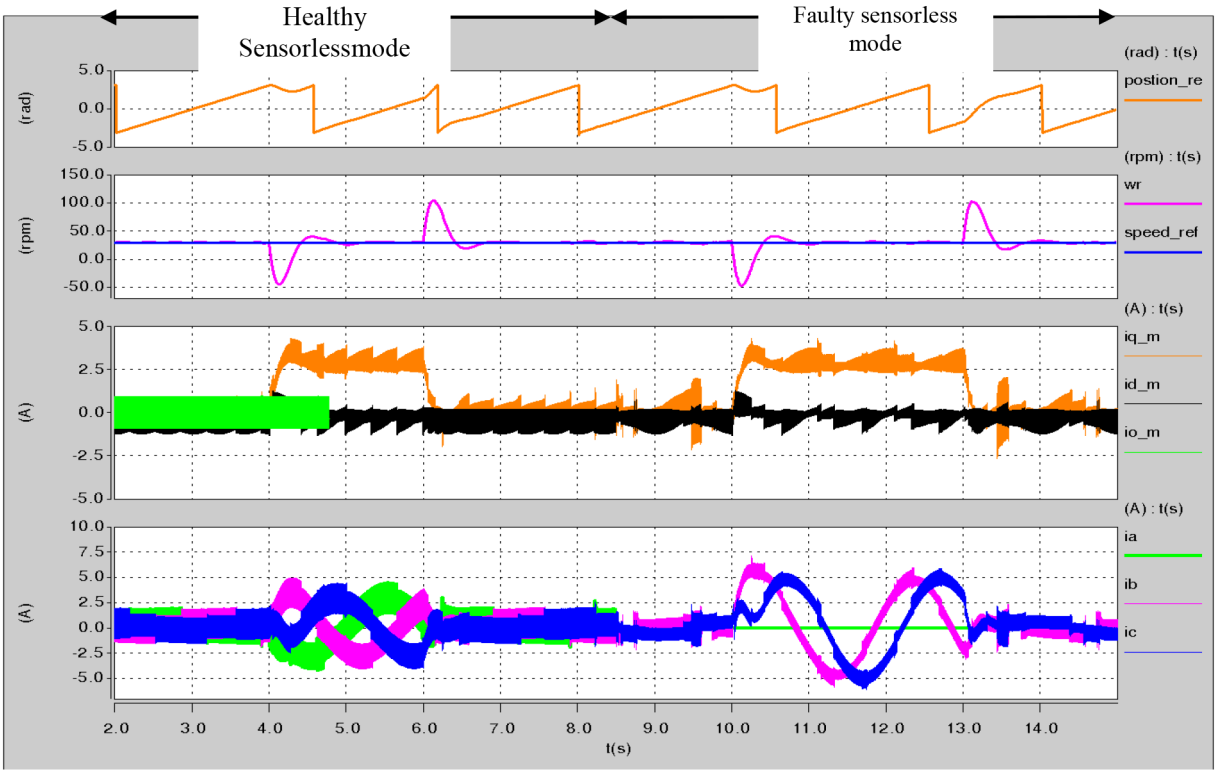

Figure 13. Fully sensorless half load steps under healthy condition and under open phase a fault condition.

7. Conclusion

This paper has outlined a new scheme for tracking the saliency of a motor fed by a 4-leg inverter in the case of a single phase open circuit fault through measuring the dynamic current response of the motor line currents due to the IGBT switching actions. The proposed method includes software modification to the method proposed in [6] to track the saliency of the motor under healthy conditions to make it applicable in the cases of open circuit phase condition. The new strategy can be used to track the saturation saliency in PM motors (2 fe) and the rotor slotting saliency in IMs (14*fr) similar to the method used in a healthy motor drive and the only difference between the PM and IM will be the tracked harmonic number. The results have shown the effectiveness of the new method in increasing the safety measures in critical systems that need continuous operation. The drawbacks of this method are increasing the total harmonic distortion of the motor's current, especially at a very low speed, due to the minimum pulse width in addition to the need for 3 di/dt sensors.

References

[1] Jansen PL, Lorenz RD. Transducerless position and velocity estimation in induction and salient AC machines. IEEE T Ind Appl 1995; 31: 240-247.

[2] Jung-Ik H, Ohto M, Ji-Hoon J, Seung-Ki S. Design and selection of AC machines for saliency-based sensorless control. In: IEEE 2002 Industrial Applications Conference; 13–18 October 2002; Pittsburgh, PA, USA. New York, NY, USA: IEEE. pp. 1155-1162.

[3] Linke M, Kennel R, Holtz J. Sensorless speed and position control of synchronous machines using alternating carrier injection. In: IEEE 2003 International Electric Machines and Drives Conference; 1–4 June 2003; Wisconsin, USA. New York, NY, USA: IEEE. pp. 1211-1217.

[4] Schroedl M. Sensorless control of AC machines at low speed and stand still based on the INFORM method. In: IEEE 1996 Industry Applications Conference; 6–10 October 1996; San Diego, CA, USA. New York, NY, USA: IEEE. pp. 270-277.

[5] Holtz J, Juliet J. Sensorless acquisition of the rotor position angle of induction motors with arbitrary stator winding. In: IEEE 2004 Industry Applications Conference; 3–7 October 2004; Washington, USA. New York, NY, USA: IEEE. pp. 1321-1328.

[6] Qiang G, Asher GM, Sumner M, Makys P. Position estimation of AC machines at all frequencies using only space vector PWM based excitation. In: IET 2006 International Conference on Power Electronics, Machines and Drives; 4–6 April 2006; Dublin, Ireland. London, UK: IET. pp. 61-70.

[7] Mendes AMS, Cardoso AJM. Fault-tolerant operating strategies applied to three-phase induction motor drives. IEEE T Ind Electron 2006; 53: 1807-1817.

[8] Bianchi N, Bolognani S, Zigliotto M, Zordan M. Innovative remedial strategies for inverter faults in IPM synchronous motor drives. IEEE T Energy Conver 2003; 18: 306-314.

[9] Meinguet F, Gyselinck J. Control strategies and reconfiguration of four-leg inverter PMSM drives in case of single-phase open circuit fault. In: IEEE 2009 Electric Machines and Drives Conference; 3–6 May 2009; Florida, USA. New York, NY, USA: IEEE pp. 299-304.

[10] Sangshin K, Taehyung K, Vodyakho O. Four-leg based matrix converter with fault resilient structure and controls for electric vehicle and propulsion systems. In: IEEE 2007 Vehicle Power and Propulsion Conference; 9–12 September 2007; Texas, USA. New York, NY, USA: IEEE. pp. 519-523.

[11] Welchko BA, Lipo TA, Jahns TM, Schulz SE. Fault tolerant three-phase ac motor drive topologies: a comparison of features, cost, and limitation. IEEE T Power Electr 2004; 19: 1108-1116.

[12] Khwan-On S, de Lillo L, Wheeler P, Empringham L. Fault tolerant four-leg matrix converter motor drive topologies for aerospace applications. In: IEEE 2010 International Symposium on Industrial Electronics; 4–7 July 2010; Bari, Italy. New York, NY, USA: IEEE. pp. 2166-2171.

[13] Gaeta A, Scelba G, Consoli A. Modeling and control of three-phase PMSMs under open-phase fault. IEEE T Ind Appl 2013; 49: 74-83.

[14] Mirafzal B Survey of fault-tolerance techniques for three-phase voltage source inverters IEEE T Ind Electron 2014; 61: 5192-5202.

[15] Viola J, Quizhpi F, Restrepo J, Pesantez JP. Analysis of a four-phase induction machine with direct torque control. In: EPE 2013 European Conference on Power Electronics and Applications; 2–6 September 2013; Lille, France. Brussels, Belgium: EPE. pp. 1-9.

[16] Nguyen-Duy K, Tian-Hua L, Der-Fa C, Hung JY. Improvement of matrix converter drive reliability by online fault detection and a fault-tolerant switching strategy. IEEE T Ind Electron 2012; 59: 244-256.

[17] Lorenz RD, Van Patten KW. High-resolution velocity estimation for all-digital, ac servo drives. IEEE T Ind Appl 1991; 27: 701-705

Appendix

The motor parameters are: rated speed = 2000 rpm, rated torque = 10.3 Nm, rated power = 2.15 kW, Kt = 2 Nm/A, Ke = 147.0 Vrms/krpm, inertia = 20.5 $kgcm^2$, R(ph-ph) = 4 Ω, and L(ph-ph) = 29.8 mH.